EFFECTS OF HEAT RELEASE ON JET FLAMES IN CROSSFLOW

E.F. Hasselbrink Jr. and M. G. Mungal
Mechanical Engineering Department
Stanford University
Stanford CA 93405–3032 USA

ABSTRACT

Two methane jets of jet-to-crossflow blowing ratios $r = 10$ and $r = 21$ are studied using particle image velocimetry in order to determine the effects of heat release on the structure of the velocity field. It is found that heat release amplifies mean velocities and RMS fluctuations by a factor as large as 2–3 compared to nonreacting cases, depending on the location in the flame. This amplification factor is seen to be quite close to the square-root of the ratio of the burned and unburned gas temperatures, and reasons for this observation are discussed.

INTRODUCTION

Many industrial combustion devices rely on jets in crossflow, also known as transverse jets, to achieve mixing and reaction. Gas turbine combustors, industrial boilers, and flare stacks, for example, use gas-phase transverse jets for injection of fuel and pollution control agents.

Recent progress has been made on the prediction of emissions of nitrogen oxides from complex systems using Advanced Reburning technology (Han et al. 1999) using a Two-Stage Lagrangian model (Broadwell and Lutz 1998) for the flow and detailed chemistry. The results depend, however, on understanding the entrainment and mixing characteristics of the flowfield, which has improved in recent years for nonreacting transverse jets (Smith and Mungal 1998; Hasselbrink and Mungal 1996). However, the results of Becker and Yamazaki (1978) and Clemens and Paul (1995) show that heat release is suspected to affect the entrainment of jet flames considerably; heat release also has a complicated influence on the turbulence properties (Takagi et al. 1981a; Takagi et al. 1981b). Furthermore, research into the effects of turbulence on the flame sheet chemistry is just beginning to document the interaction of strain and vorticity with reaction zones (Rehm and Clemens 1999).

Previous studies have investigated free or coflowing jet flames; however, a common industrial configuration for burners and boilers is the jet in a crossflow, also known as the transverse jet. The behavior of the transverse jet is largely parameterized by the blowing ratio, r, defined as

$$r \equiv \left(\frac{\rho_j u_j^2}{\rho_\infty \overline{u}_\infty^2} \right)^{1/2} \tag{1}$$

where u_j is the effective jet exit velocity (defined as the equivalent uniform jet exit velocity with the same momentum flux). The goal of the present work is to document the effects of heat release on this complex flow, in particular on its mean flowfield and turbulent fluctuations.

EXPERIMENTAL SYSTEM

Flow Facility

The flow facility is a low-speed indraft aluminum wind tunnel used in a previous investigation (Smith and Mungal 1998), with minor changes. The tunnel has a 50×50 cm cross-section and rounded inlet with 2.5:1 contraction ratio. Optical access is afforded by a large $50 \times 80 \times 0.63$ cm Pyrex window on one side, a $15 \times 15 \times 0.95$ cm quartz window on the opposite side, and a $5 \times 25 \times 0.4$ cm quartz window on the wall opposite the jet exit for laser access. Honeycomb and screens at the inlet ensure that turbulence intensity is less than 1%, and mean velocity is uniform to within 5%, across the region impinging on the jet.

The jet is injected normal to the crossflow through a 25 cm long tube (6.35 mm OD, 4.72 mm ID, 316 stainless steel), protruding 7 cm into the wind tunnel. The main jet tube is located within an annular tube (9.5 mm

OD) which issues a hydrogen pilot. In the absence of this hydrogen pilot flame, the flame lifts several centimeters from the jet. In the present experiments, the jet is always used in the unpiloted configuration.

In reacting experiments, the jet and crossflow are both seeded with 0.3 μm (nominal) alumina (Al_2O_3) particles, using stirred fluidized-bed seeders. Conical cyclones are also employed to remove large agglomerates of particles. Designs for the seeder and cyclone were based on published design rules (Cheremisinoff and Cheremisinoff 1984; Nichols 1985). In nonreacting experiments, the jet is seeded with alumina, but the crossflow is seeded with 0.3 μm glycerol fog particles from a theatrical fog generator.

PIV System

The PIV system hardware in this study consists of (1) a dual-cavity Nd:YAG laser (Spectra Physics PIV-400, 320 mJ pulse at 532 nm, 15 Hz double-pulse repetition rate), (2) high reflectivity 532 nm dichroic mirrors and sheet forming optics, and (3) a high resolution interline frame transfer CCD camera (1000 × 1000 9-μm pixel array, Kodak ES-1.0, 60% fill factor) with 105 mm Nikkor lens at f/5.6, mounted on a tilt/rotation stage (Newport Series 36), connected to a personal computer with a fast PCI frame grabber (provided by TSI, Inc.).

PIV image processing is performed with a custom two-frame FFT cross-correlation algorithm using recursive interrogation region offset. This method is employed in order to minimize in-plane "loss-of-correlation" (Westerweel et al. 1997; Westerweel 1997). In this way, the integer displacement in the correlation plane is always zero, and the probability of valid vector detection is independent of particle displacement; hence detectability is maximized (Raffel et al. 1998), which is important in the low-density (high temperature) regions of turbulent flames. A simple "tent map" correction for the loss-of-correlation function is employed to reduce bias error. In-depth discussion of the algorithm is given elsewhere (Hasselbrink 1999). Typical interrogation region size (final pass) is 32 pixels. Magnification used in the present work is either 37 pixels/mm or 19 pixels/mm.

Once an ensemble of instantaneous vector fields have been obtained from a set of images, the raw data are cast from pixel units into physical coordinates, and turbulence statistics and derived quantities such as vorticity and strain rate are calculated, using custom software which has also been documented elsewhere (Urban 1999).

Experimental Conditions

Four cases are studied: $r = 10$ and $r = 21$ (nominal) nonreacting jets, and $r = 10$ and $r = 21$ flames. In all cases, the jet was comprised of 99.0% methane. Corresponding Reynolds numbers are 6300 and 12 600.

TABLE 1: EXPERIMENT CONDITIONS.

Parameter	Case $r = 10$ (nom)	Case $r = 21$ (nom)
Actual r	10.0 ± 2%	21.4 ± 3%
u_j [m/s]	21.3	45.5
Re	6000	12800
$\bar{u}_\infty$ [cm/s]	157.5 ± 1.5	157.5 ± 2.7
L_f/d	59	64
$\xi_L = \mathrm{Ri}^{1/3} L_f/d$	2.7	1.8
L_{mom}/d	32	54

A summary of the experimental conditions is shown in Table 1. Included in this table is a listing of the flamelength, L_f. Also included is the buoyancy length scale of Becker and Yamazaki (1978), $\xi_{L_f} = \mathrm{Ri}^{1/3} L_f/d$, where $\mathrm{Ri} = gd/u_j^2$ is the Richardson number. If ξ_{L_f} is less than about 1.5, buoyancy is considered negligible. A lengthscale L_{mom} can be defined such that $\xi_{L_{mom}} = 1.5$, which denotes the distance along the flame over which buoyancy is unlikely to be a major influence on the flow. By comparing L_{mom} with L_f it seems that buoyancy has a moderate effect on the $r = 10$ case, and probably only a mild effect on the $r = 21$ case. We note, however, that Becker & Yamazaki's results were obtained for free jets, and hence may not be directly applicable to the transverse jet. Mie-scattering images comparing a nonreacting jet and jet flame are shown in Figure 1. A pulsed sheet of laser light from a Nd:YAG laser illuminates glycerol fog particles seeded into the crossflow or alumina particles seeded into the jet. The visualization shows that the turbulent scales in the wake behind the jet are significantly more laminar than the turbulence within the jet. This behavior appears to be a symptom of the additional complication created by the crossflow: it is possible to define two Reynolds numbers for the flow, one based on the jet velocity, and one based on crossflow velocity.

Maintaining a flame envelope around the entire jet has not proven to be possible for the scale of the present experiments, even with the use of a hydrogen pilot (Hasselbrink and Mungal 1998). This behavior is markedly different from the behavior of lifted co-flowing flames, where the addition of a hydrogen pilot usually attaches the flame to the jet nozzle, and thereby prevents any premixing of fuel and air (Muñiz 1999). For this reason, the simpler unpiloted case was selected for detailed velocity field measurements.

Imaging Locations

A mosaic of small imaging windows have been used to construct images of the overall flowfield, in order to obtain reasonable measurement resolution. Two sizes of imaging windows are used: the high resolution window,

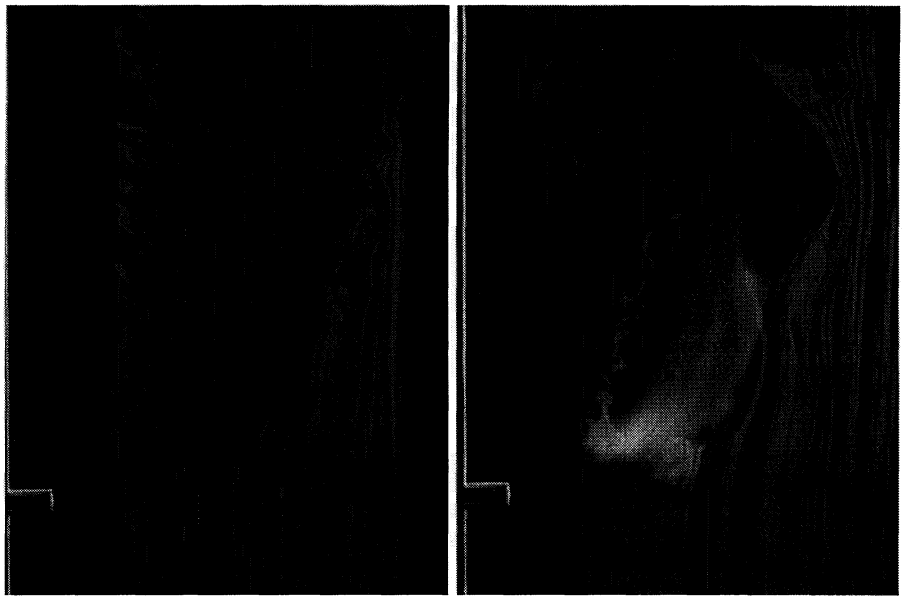

Figure 1: Mie-scattering visualization photographs. Left, nonreacting methane jet. Right, methane flame.

used in the near field, is approximately 2.5 cm square, while the low resolution window used elsewhere is approximately twice this size. The vector grid is 64×64 (32-pixel interrogation regions, 1008×1016 format camera), representing 50% interrogation region (IR) overlap. Although the PIV grid spacing is 5 times larger than the smallest viscous scale of the flow (using estimates from (Dowling and Dimotakis 1990), we can expect to capture about 83% of the fluctuation energy in each component based on the free-jet turbulence spectrum (Champagne 1978).

RESULTS

Flow Structure

Grayscale colormaps of the $\overline{u}$ and $\overline{v}$ fields are compared for the $r = 10$ jet and flame in Figures 2–3. The center streamline, integrated for each case from the center of the jet nozzle, is shown for reference.

In the nonreacting jet, the $\overline{v}$ contours show that the crossflow slows as it approaches the jet, but then increases to values greater than v_∞ along the centerline trajectory. Values of $\overline{v}$ behind the jet are less than the crossflow velocity; in the lee of the near-field flow in fact, strong reverse flow with $\overline{v} = -1.2v_\infty$ occurs, indicating strong entrainment into the jet. Overall, we note that the jet introduces a deficit of momentum in the y-direction, so that $\int_A \overline{v}(v_\infty - \overline{v})dA < 0$.

In the jet flame, the contours of $\overline{u}$ show that the flame influences the exterior flowfield at surprisingly large distances away from the heated region (note, however, that the grayscale map is highly skewed towards small values of u, in order to emphasize the structure of the jet). Contours of $\overline{v}$ also show dramatic increases in the heated regions of the flow. In the far-field of the nonreacting jet, $\overline{v} \to v_\infty$, but in the flame, $\overline{v} \to 2.5v_\infty$.

The u'_{rms} fields for the reacting and nonreacting cases are compared in Figure 4. Interestingly, the locus of maximum RMS fluctuation corresponds quite well to the center streamline integrated from the nozzle exit, in spite of the fact that the locus of maximum $\overline{u}$ does not.

These results can be better understood by considering only the *characteristic* (*i.e.*, centerline) velocities and fluctuation magnitudes. Furthermore, the effects of heat release can be isolated by properly accounting for the effects of r. It has been suggested (Hasselbrink and Mungal 1996) that characteristic velocities and scalar concentrations of nonreacting jets obey a scaling law in the region $y/rd > 1$ which shows the same power-law dependence on y as an axisymmetric wake:

$$\frac{\overline{u}_c}{u_j} \sim \frac{v_\infty - \overline{v}_c}{v_\infty} \sim \overline{\xi} \sim \frac{1}{r}\left(\frac{\rho_j}{\rho_\infty}\right)^{\frac{1}{2}}\left(\frac{y}{rd}\right)^{-\frac{2}{3}} \quad (2)$$

Here the subscript c is used to denote values at the centerline. In the region closer to the jet nozzle, Hasselbrink (1999) has shown that a jet-like region exists, where

$$\frac{\overline{u}_c}{u_j} \sim \overline{\xi} \sim \left(\frac{\rho_j}{\rho_\infty}\right)^{\frac{1}{2}}\left(\frac{x}{rd}\right)^{-1} \sim \left(\frac{\rho_j}{\rho_\infty}\right)^{\frac{1}{2}}\left(\frac{y}{rd}\right)^{-\frac{1}{2}} \quad (3)$$

These scaling laws suggests that the characteristic ru/u_j should collapse to a single curve when plotted

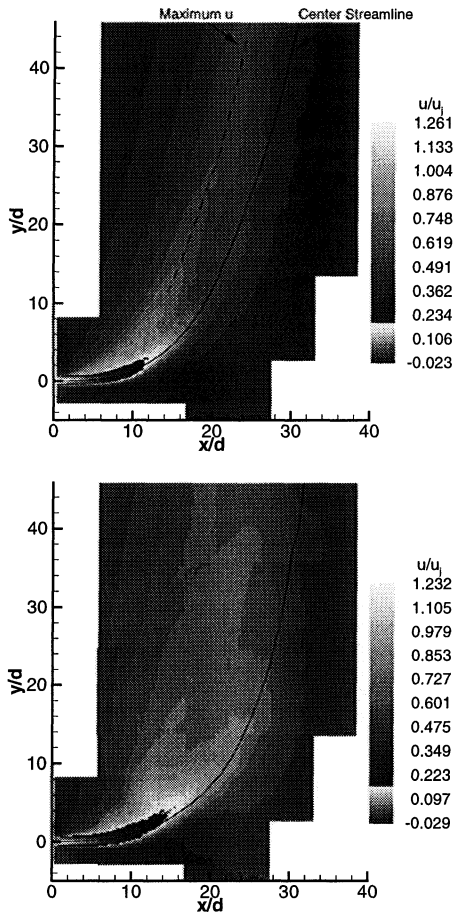

Figure 2: Grayscale contour maps of $\mathbf{u/u_j}$, $\mathbf{r = 10}$ case. Top, nonreacting methane jet. Bottom, methane flame.

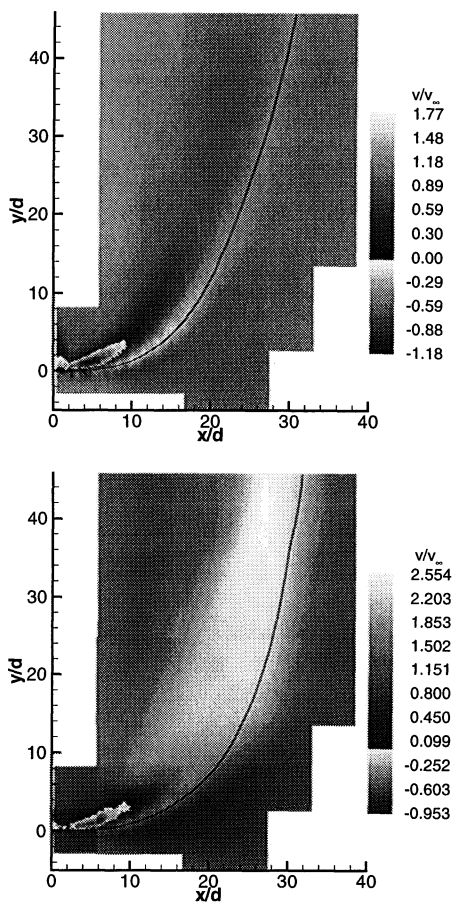

Figure 3: Grayscale contour map of $\mathbf{v/v_\infty}$, $\mathbf{r = 10}$ case. Top, nonreacting methane jet. Bottom, methane flame.

against y/rd. Figure 5 plots the data in this similarity coordinate system, and shows that the nonreacting jets (solid symbols) do in fact collapse to a single curve. The scaling laws for the jet-like and wake-like regions are shown for comparison. Agreement is very good in the near-field, but less so in the far-field. It is suspected that the disagreement in the far field stems from the fact that the maximum u does not fall along the center streamline, as shown in Figure 2. At any rate, the effects of heat release are clearly shown in the differences between the solid and open symbols, which correspond to methane flame cases. Heat release amplifies the u component by a factor of up to two over the nonreacting cases.

The effect of heat release on the turbulence fluctuations is similar to the effects on the mean field. Assuming that fluctuations are in constant proportion to local velocity differences, it is expected that they should also scale as given in Eq. 2–3. RMS u' fluctuations are plotted in these similarity coordinates in Figure 6. This time, the agreement with both scaling laws is very good for the nonreacting cases. There is a sharp increase in RMS fluctuation starting at the flame base location, and the amplification increases further along the flame, up to a factor of about 2.4 over the nonreacting case.

DISCUSSION

A recurring theme for the effects of heat release on this flow is that velocities and fluctuations are amplified by a factor between 2 and 3, with a typical value near 2.5. This value seems quite close to $(T_b/T_u)^{1/2}$, where T_b and T_u are the unburned and burned fluid temperatures, respectively. For methane flames at stoichiometry, the adiabatic flame temperature is $T_{af} = 2260\,\mathrm{K}$, so the square-root of the temperature ratio is approximately 2.7. The peak mean temperature in the flame is expected to be somewhat lower than T_{af}, however, due

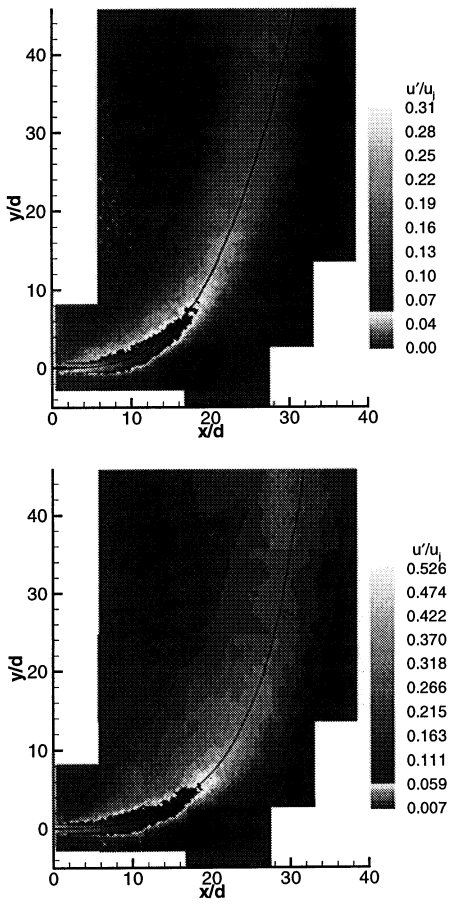

Figure 4: Grayscale contour maps of $\mathbf{u'_{rms}/u_j}$, $\mathbf{r = 10}$ case. Top, nonreacting methane jet. Bottom, methane flame.

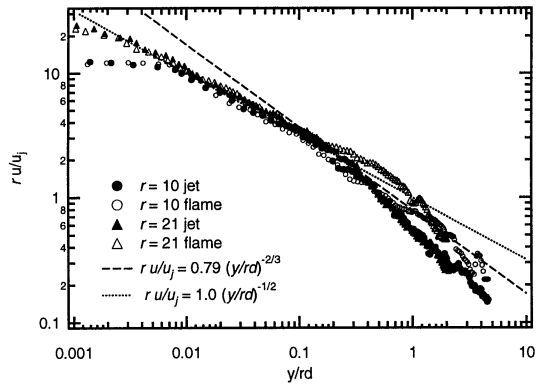

Figure 5: $\mathbf{r\bar{u}/u_j}$ vs $\mathbf{y/rd}$ along the jet center streamline.

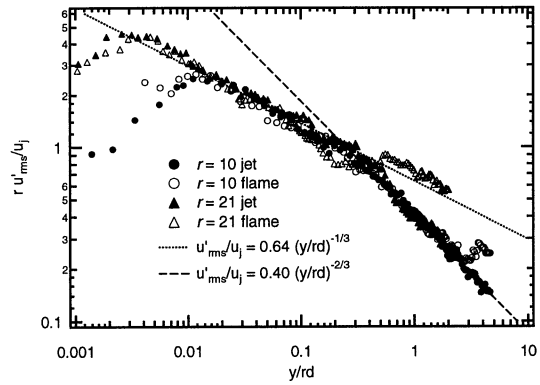

Figure 6: $\mathbf{ru'_{rms}/u_j}$ vs $\mathbf{y/rd}$ along the transverse jet center streamline.

to fluctuations and due to radiative energy losses.

According to the Rankine-Hugoniot relations for a 1-dimensional steady flame, mass conservation requires that the flowspeed ratio $u_b/u_u = T_b/T_u$ (under the ideal-gas approximation). Our finding, which can be idealized as $u_b/u_u = (T_b/T_u)^{1/2}$, implies that the effect of heat release in jets is quite different from the 1D case; in these flames, the upstream flow is free to move around the region of heat release, *i.e.*, the region of heat release is finite. Ruetsch et al. (1995) analyzed the velocity field in the vicinity of a laminar triple flame, which results when a flame propagates through the flammable layer in a region with a mixture fraction gradient. Although their analysis is concerned primarily with the propagation speed of the flame, it is noted that $u_b \sim (T_b/T_u)^{1/2} S_L$, where S_L is the laminar flame speed. The difference in behavior from a 1D flame is attributed to the divergence of streamlines in the flow approaching the flame, caused by the curvature of the flame front. We note that their analysis, however, makes no presumptions that the flame assumes a triple-flame structure; it merely presumes a finite region of heat release, unconfined flow (*e.g.*, no walls), and negligible influence of pressure. It is therefore believed that this analysis is, in some ways, applicable to the jet in the large scale, as well as in the smaller scale of the flame base region.

CONCLUSIONS

- In both reacting and non-reacting jets, the locus of maximum $\overline{u}$ corresponds to the jet center streamline trajectory in the near-field, but not the far field. The locus of maximum $\overline{v}$ and RMS fluctuations, however, follow the center streamline trajectory quite well. As the crossflow approaches the leading edge of the jet, it is slowed significantly on the windward side of the jet near-field region.

Strong reverse flow occurs in the lee side of the jet.

- Scaling laws provide a reasonably good framework for predicting the form of the streamline trajectory and the evolution of the fluctuation amplitudes along that trajectory. Because maximum u does not follow the streamline trajectory in the far-field, the scaling laws are less accurate for this flowfield variable. The crossflow (v) component of velocity relaxes rapidly to the crossflow speed in the absence of combustion heat release.

- Combustion heat release accelerates the flow within the heated region. As the flame tip is approached, maximum $\overline{v}/v_\infty \approx 2.7$. Since, in the nonreacting case, $\overline{v}/v_\infty \rightarrow 1$, this suggests $\overline{v}_{flame}/\overline{v}_{no\ flame} \approx \left(\frac{T_b}{T_u}\right)^{1/2}$. A similar amplification factor is observed for both $\overline{u}$ and the RMS turbulent fluctuations.

ACKNOWLEDGMENTS

The authors gratefully acknowledge the assistance of Dr. Lester Su, Mr. Donghee Han, and Mr. Raymond Miraflor in the experimental work, and for many discussions regarding the results. We also acknowledge the support of Gas Research Institute contract no. 5093-260-2697 and R. V. Serauskas, Technical Monitor.

REFERENCES

Becker, H. A. and S. Yamazaki (1978). Entrainment, momentum flux and temperature in vertical free turbulent diffusion flames. *Combustion and Flame 33*, 123–149.

Broadwell, J. E. and A. E. Lutz (1998). A turbulent jet chemical reaction model: NO_x production in jet flames. *Combustion and Flame 114*(3/4), 319–335.

Champagne, F. H. (1978). The fine-scale structure of the turbulent velocity field. *Journal of Fluid Mechanics 86*, 67–108.

Cheremisinoff, N. P. and P. N. Cheremisinoff (1984). *Hydrodynamics of Gas-Solids Fluidization.* Gulf Publishing Company.

Clemens, N. T. and P. H. Paul (1995). Effects of heat release on the near field flow structure of hydrogen jet diffusion flames. *Combustion and Flame 102*(3), 271–284.

Dowling, D. R. and P. E. Dimotakis (1990). Similarity of the concentration field of gas-phase turbulent jets. *Journal of Fluid Mechanics 218*, 109–141.

Han, D. H., M. G. Mungal, V. M. Zamansky, and T. J. Tyson (1999). Prediction of NO_x control by basic and advanced gas reburning using the two-stage lagrangian model. *Combust. and Flame, to appear.*

Hasselbrink, E. F. (1999). *Transverse Jets and Jet Flames: Structure, Scaling, and Effects of Heat Release.* Ph. D. thesis, Mechanical Engineering Department, Stanford University.

Hasselbrink, E. F. and M. G. Mungal (1996). An analysis of the time-averaged properties of the far field of the transverse jet. Paper No. 96-0201, AIAA 34th Aerospace Sciences Meeting.

Hasselbrink, E. F. and M. G. Mungal (1998). Observations on the stabilization region of lifted nonpremixed methane transverse jet flames. In *Twenty-Seventh Symposium (International) on Combustion*, Boulder, CO. The Combustion Institute, Pittsburgh, USA.

Muñiz, L. (1999). *Particle Image Velocimetry Studies of Turbulent Nonpremixed Flames.* Ph.D. thesis, Stanford University.

Nichols, C. E. (1985). Experiments with solid particle seeding. In W. W. Hunter and C. E. Nichols (Eds.), *NASA CP 2393: Wind Tunnel Seeding Systems for Laser Velocimeters*, pp. 77–84.

Raffel, M., C. Willert, and J. Kompenhans (1998). *Particle Image Velocimetry, A Practical Guide.* Berlin: Springer-Verlag.

Rehm, J. E. and N. T. Clemens (1999). The large-scale turbulent structure of nonpremixed planar jet flames. *Combustion and Flame 116*, 615–626.

Ruetsch, G., L. Vervisch, and A. Liñan (1995). Effects of heat release on triple flames. *Physics of Fluids 7*(6), 1447.

Smith, S. H. and M. G. Mungal (1998). Mixing, structure and scaling of the jet in crossflow. *Journal of Fluid Mechanics 357*, 83–122.

Takagi, T., H.-D. Shin, and A. Ishio (1981a). Local laminarization in turbulent diffusion flames. *Combustion and Flame 37*, 103–170.

Takagi, T., H.-D. Shin, and A. Ishio (1981b). Properties of turbulence in turbulent diffusion flames. *Combustion and Flame 40*, 121–140.

Urban, W. D. (1999). *Planar Velocity Measurements in Compressible Mixing Layers.* Ph.D., Stanford University.

Westerweel, J. (1997). Fundamentals of particle image velocimetry. *Measurement Science and Technology 8*(12), 1379–1392.

Westerweel, J., D. Dabiri, and M. Gharib (1997). The effect of discrete window offset on the accuracy of cross-correlation analysis of digital PIV recordings. *Experiments in Fluids 23*(1), 20–28.